Stress-induced seismic velocity anisotropy and physical properties in the SAFOD Pilot Hole in Parkfield, CA

Naomi L. Boness and Mark D. Zoback

Department of Geophysics, Stanford University, California, USA

[1] A comprehensive suite of geophysical logs was collected in the SAFOD Pilot Hole from a depth of 775 m to 2150 m in highly fractured Salinian granite. The Pilot Hole intersected numerous macroscopic fractures and faults with extremely varied orientations. Despite the highly variable orientation of the fractures and faults, the fast polarization direction of the shear waves is very consistent with the direction of maximum horizontal compression determined from wellbore breakouts and drilling induced tensile fractures. At least three major shear zones were intersected by the borehole that are characterized by anomalously low velocity and resistivity, anomalously high shear velocity anisotropy and an absence of stress-induced wellbore breakouts (which suggests anomalously low differential stress). We argue that the physical mechanism responsible for the seismic velocity anisotropy observed in the Pilot Hole is the preferential closure of fractures in response to an anisotropic stress state. *INDEX TERMS:* 0915 Exploration Geophysics: Downhole methods; 5102 Physical Properties of Rocks: Acoustic properties; 7205 Seismology: Continental crust (1242); 8150 Tectonophysics: Plate boundary—general (3040). **Citation:** Boness, N. L., and M. D. Zoback (2004), Stress-induced seismic velocity anisotropy and physical properties in the SAFOD Pilot Hole in Parkfield, CA, *Geophys. Res. Lett.*, *31*, L15S17, doi:10.1029/2003GL019020.

1. Introduction

[2] In the summer of 2002 the Pilot Hole for the San Andreas Fault Observatory at Depth (SAFOD) was drilled to a depth of 2.15 km through 768 m of tertiary sediments and into Salinian granite. Data from the Pilot Hole provides a unique opportunity to measure the physical properties of the shallow crust adjacent to the San Andreas Fault. In this paper we present shear wave velocity anisotropy observations and correlate them with measurements of P- and S-wave velocity, resistivity, density and porosity, the distribution of faults and fractures intersecting the borehole and the state of stress inferred from borehole measurements.

2. Faults, Fractures and Rock Properties

[3] The right lateral, strike-slip San Andreas Fault is the dominant structural feature in the Parkfield region. Secondary, strike-slip and shallow thrust faults with a sub-parallel northwest-southeast trend also occur throughout the area. Based on studies of P-wave velocity determined from a seismic reflection/refraction profile [*Catchings et al.*, 2002]

and interpretation of potential field data (R. Jachens, personal communication, 2003) it was anticipated that the Pilot Hole would encounter fractured granite beneath ~750 m of Tertiary and Quaternary sedimentary rocks; the fractured Salinian granite was encountered at 768 m. A comprehensive suite of geophysical logs was collected in the fractured granite from a depth of 775 m to 2150 m. P-and S-wave sonic velocity, electrical resistivity, gamma ray, and density were recorded over the entire depth range at a 15 cm sampling interval. Figure 1 shows these data after applying a 3 m running average to the logs. Electrical and ultrasonic image logs were also acquired in the borehole to facilitate an analysis of the fractures and faults intersected by the borehole as well as stress-induced wellbore failures such as breakouts and drilling-induced tensile cracks.

[4] As expected, the Pilot Hole velocity logs show an overall increase in P- and S-wave velocity with depth (Figure 1). The compressional wave velocity, V_p, ranges from approximately 5 km/s at a depth of 775 m to 5.65 km/s at a depth of 2150 m. Similarly, the shear wave velocity, V_s, ranges from 2.8 km/s to 3.25 km/s. Both the P- and S-wave data reveal the presence of anomalously low velocity zones. These include intervals at 1150–1200 m, 1310–1420 m and 1835–1880 m that correlate with regions of intense fracturing (see below). We also note that the V_p/V_s ratio has an average value of 1.7 (equivalent to a Poisson's ratio, υ, of 0.24) but in the three intervals of lower velocity this ratio increases. This increase is especially prominent within the low velocity zones at 1310–1420 m and 1835–1880 m, where V_p/V_s reaches its maximum value of approximately 1.9 ($\upsilon = 0.3$).

[5] Overall, densities in the Pilot Hole increase with depth from approximately 2.5 g/cm^3 to 2.7 g/cm^3, which is expected for rock with granitic composition. Porosity values, determined from the density log, are between 2 and 15% for most of the log, indicating highly fractured granite. Within the interval 1150–1200 m there is a decrease in density and a corresponding increase in porosity. At a depth of 1400 m there is a 5% decrease in porosity and a simultaneous density increase of 0.2 g/cm^3. Porosity decreases by a further 2% at a depth of 1850 m and density increases to a value of 2.65 g/cm^3, which remains virtually constant to the bottom of the well.

[6] Resistivity increases with depth in the Pilot Hole from about 30 ohm-m at 800 m depth to 1000 ohm-m at the bottom of the borehole (Figure 1), an order of magnitude lower than those associated with laboratory measurements of intact crystalline rock [*Pezard and Luthi*, 1988; *Zablocki*, 1964]. *Unsworth et al.* [2000] determined the resistivity structure along a profile through the drill site by modeling surface magnetotelluric data. We find reasonable agreement between the log data and this model (both shown in
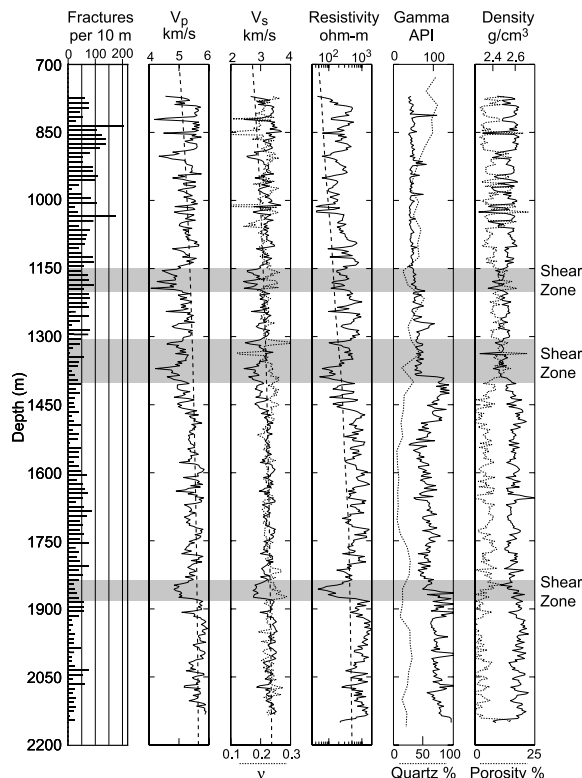
Figure 1. Distribution of macrofractures intersected by the Pilot Hole as determined from the FMI log and physical property logs acquired in the Pilot Hole averaged over 3 m depth intervals. Dashed lines on the seismic velocities indicate gross trends with depth and the dashed line on the resistivity is the model determined by *Unsworth et al.* [2000]. Intervals of the borehole with significantly anomalous physical properties, interpreted to be major shear zones, are highlighted.

Figure 1), although *Unsworth et al.*'s [2000] model seems to slightly under predict the resistivity at depth. Two of the intervals noted above (1310–1420 m and 1835–1880 m) have resistivities that are significantly lower than the overall trend with depth. The resistivity of fractured crystalline rock is very sensitive to the presence of interstitial fluids [*Brace et al.*, 1965; *Brace and Orange*, 1968; *Brace*, 1971] and alteration minerals [e.g., *Palacky*, 1987]. As the porosity shows no significant increase in these zones we assume the low resistivity is a result of the mineralogy.

[7] Variations in gamma ray radiation are often associated with changes in lithology, particularly the presence of clay minerals and an increase in feldspar. The gamma ray log from the Pilot Hole shows an overall increase in the amount of radiation with depth from about 25 to 75 API units. We observe two significant increases in the gamma radiation (over 50 API units) at depths of approximately 1400 m and 1850 m. These variations are associated with significant decreases in the amount of quartz, increases in the amount of feldspar, clay minerals and oxides as determined from mineralogical point counts of cuttings collected in the Pilot Hole during the drilling phase (M. Rymer, personal communication, 2003) The intervals at 1310–1420 m and 1835–1880 m are also associated with significant increases in the

thermal conductivity [*Williams et al.*, 2004] and large increases in the magnetic susceptibilities [*McPhee et al.*, 2004]. An increase in gas emissions was recorded at the time of drilling as each of the intervals at 1150–1200 m, 1310–1420 m and 1835–1880 m was penetrated [*Erzinger et al.*, 2004], although elevated pore pressure was not observed.

[8] The distribution and orientation of macroscopic faults and fractures intersected by the Pilot Hole was obtained by analyzing data from a Formation Micro Imager (FMI) log [*Ekstrom et al.*, 1987] acquired in the Pilot Hole. The abundance of macroscopic faults and fractures decreases from approximately 125 per 10 m interval in the upper section of the log (Figure 1) to about 25 per 10 m interval at the bottom of the borehole. There are several intervals where the granite is so highly faulted and fractured that the number of individual features within each of these zones is impossible to ascertain. The most prominent of these intervals are between 1150–1200 m, 1310–1420 m and 1835–1880 m, the same intervals with anomalous geophysical properties described above. No preferential orientation of macrofractures is observed at any depth as can be seen in the lower hemisphere stereographic projections of the fractures over 150 m intervals shown in Figure 2 (and determined statistically).
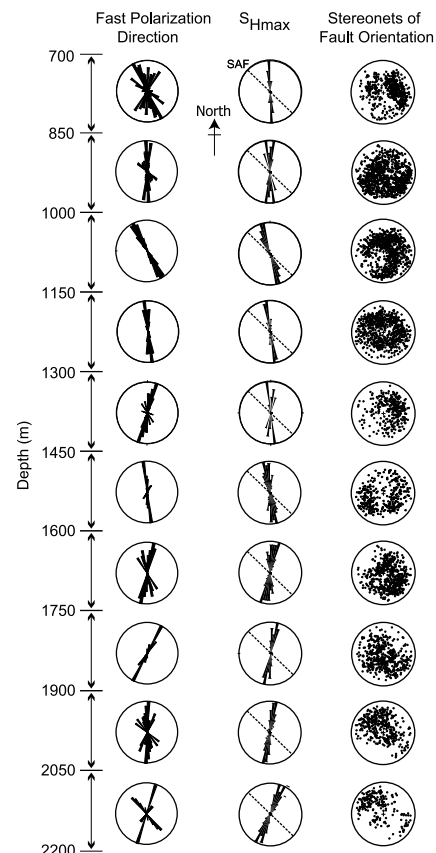
Figure 2. Comparison of the fast shear polarization direction with S_{Hmax} determined from borehole breakouts and tensile cracks [*Hickman and Zoback*, 2004] and fracture orientations as observed on the FMI log. The strike of the San Andreas Fault (SAF) is shown for reference. The direction of the fast shear direction correlates very well with the orientation of S_{Hmax} whereas the distribution of fracture orientations is seemingly random.

[9] We hypothesize that the anomalous intervals noted above (1150–1200 m, 1310–1420 m and 1835–1880 m) are associated with major shear zones cutting across the borehole. In addition to having anomalous geophysical properties and an extremely high number of fractures and faults, these zones are hydraulically conductive (as indicated by the increase in gases) and thus appear to be active faults [*Barton et al.*, 1995; *Townend and Zoback*, 2000]. The high Vp/Vs ratio in these intervals is indicative of increased microcracks [*Moos and Zoback*, 1983] and/or materials with a low shear modulus. However, the porosity log does not reveal high porosity confined within any of the anomalous intervals, but rather shows a step in density/porosity indicating a change of lithology. These step changes in density/porosity are correlated with analogous steps in gamma ray radiation values implying a change of lithology across the fault(s) in the shear zones.

3. Seismic Velocity Anisotropy

[10] Data from a Dipole Sonic Shear Image (DSI) log [e.g., *Chen*, 1988; *Mueller et al.*, 1994] acquired in the Pilot Hole is used to assess shear wave velocity anisotropy. The DSI tool consists of a relatively low frequency source (0.8–5 KHz), which causes a flexing of the borehole wall that, in turn, directly excites shear waves penetrating approximately 1.5 m into the formation. The flexural wave is dispersive with low frequencies having a large penetration depth and reflecting shear velocities away from the wellbore. The effect of stress concentrations around the borehole is removed by filtering out the high frequencies that correspond to penetration depths of less than 3 borehole radii (equivalent to about 67 cm for the Pilot Hole).

[11] The results of the shear wave anisotropy analysis are shown in Figure 2 with the fast polarization directions shown for ten discrete 150 m intervals of the borehole. The amount of velocity anisotropy (defined as $100(Vs_1 - Vs_2)/Vs_1$, where Vs_1 is the fastest shear velocity and Vs_2 is the slower velocity) is averaged over 3 m intervals and found to decrease with depth from approximately 10% at 775 m to 3% at 2150 m (Figure 3). We ensure data quality of the dipole shear wave data by requiring the following: 1) A velocity anisotropy greater than 2%; 2) An energy difference between the fast and slow waves of more than 50%; 3) A minimum energy greater than 15%. We observe intervals in the Pilot Hole, where anisotropy appears to increase significantly above the overall trend. For example, in the interval of 1310–1420 m the amount of anisotropy increases from approximately 4% to 11%. This phenomenon is also observed clearly between depths of 1835 and 1880 m (Figure 3). Caliper measurements of borehole diameter indicate that this increase in anisotropy is not an artifact due to borehole shape or size.

[12] There are five known causes of shear wave anisotropy in the crystalline crust [see reviews by *Crampin et al.*, 1984; *Crampin*, 1987; *Crampin and Lovell*, 1991]: 1) Anisotropic in situ stresses cause the preferred closure of fractures at all scales in a highly fractured crust, thus generating a fast direction parallel to S_{Hmax}; 2) Dilatancy of stress-aligned fluid-filled microcracks that also produce a fast direction aligned with S_{Hmax}; 3) Alignment of macroscopic fractures without stress effects; 4) The direct effect of
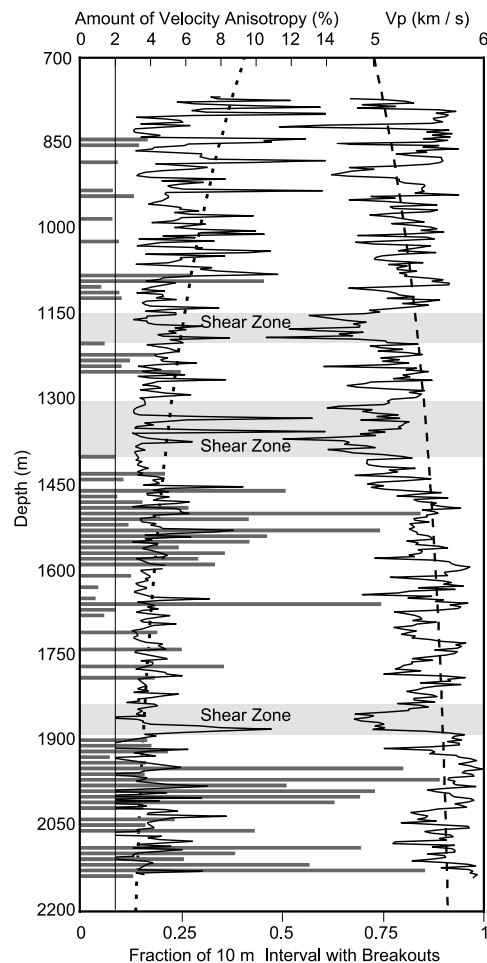
Figure 3. Fraction of the Pilot Hole with borehole breakouts shown as a bar graph with the amount of velocity anisotropy and P-wave sonic velocity superimposed. The highlighted shear zones are associated with high amounts of velocity anisotropy that correlate with an absence of borehole breakouts and low sonic velocity indicating the presence of stress relief zones.

an anisotropic stress field on the elastic properties of intact rock; and 5) Alignment of minerals or grains.

[13] Our observation of randomly oriented macroscopic fractures and faults cutting across the Pilot Hole (Figure 1) leads us to believe that we can eliminate aligned macroscopic fractures as the cause of the shear wave anisotropy since the fast polarization directions show a consistent orientation (Figure 2). In direct contrast, the direction of maximum horizontal compression, S_{Hmax}, from stress-induced wellbore breakouts and drilling-induced tensile cracks [*Hickman and Zoback*, 2004] correlates very well with the fast polarization directions of the shear waves (Figure 2). Note the correlation of the fast polarization direction and S_{Hmax} at all depths: From 850–1000 m both the fast direction and S_{Hmax} are approximately north–south, from 1000–1600 m the orientations both rotate to slightly east of north and below a depth of 1600 m both the fast direction and S_{Hmax} are east of north.

[14] Direct stress-induced anisotropy is improbable since the deviatoric stresses in the Earth are orders of magnitude smaller than those required to produce the observed amount

of velocity anisotropy [*Dahlen*, 1972]. We also eliminate aligned minerals and grains as a cause of the observed anisotropy since the Pilot Hole cuttings showed no evidence of aligned minerals or grains.

[15] The alignment of fluid-filled microcracks in response to the stress field, commonly known as Extensive Dilatancy Anisotropy (EDA) [*Crampin et al.*, 1984; *Crampin*, 1987], is widely hypothesized as the cause of crustal shear wave anisotropy. However, note that the amount of velocity anisotropy increases in regions where breakouts are absent (Figure 3). While the lack of borehole breakouts could be due to either high rock strength, or locally low differential stress, we observe that the sonic velocities are low in the regions without breakouts (Figure 3), indicating that the rock strength is not anomalously high in these intervals and that these are indeed stress relief zones [*Hickman and Zoback*, 2004]. The increase in velocity anisotropy in the intervals containing few breakouts results from an increase in the sensitivity of seismic velocity. We hypothesize that this is either due to low mean stress magnitudes [*Nur and Simmons*, 1969] or an increase in microcracking [*Moos and Zoback*, 1983]. As the high anisotropy zones also correlate in depth with the intervals of the Pilot Hole interpreted as major shear zones from the petrophysical data, slip on faults within these zones [*Hickman and Zoback*, 2004] would explain both local stress drops and an increased amount of microcracking. It should be noted that these observations are not consistent with EDA since microcrack dilatancy requires high differential stress that would promote breakout formation, contradictory to our observations. All things considered, the most viable model for the seismic anisotropy of the crust in this region is that the anisotropic stress field causes the preferred closure of fractures at all scales in an essentially randomly fractured crust. The decrease in the number of fractures with depth explains the decrease in the amount of velocity anisotropy.

4. Summary

[16] Using geophysical logs from the SAFOD Pilot Hole we have characterized the variation of physical properties with depth within the Salinian granite. We find that P- and S-wave velocity and density increase with depth while the number of faults and fractures in the rock and shear wave velocity anisotropy decreases. There is an excellent correlation between the fast polarization direction of the shear waves and the direction of maximum horizontal compression as determined from borehole breakouts. We interpret three intervals of anomalous physical properties at depths of 1150–1200 m, 1310–1420 m and 1835–1880 m as major shear zones. These intervals are associated with anomalously low sonic velocities and high shear velocity anisotropy. The absence of breakouts in these intervals (even though the materials are almost certainly weaker than the surrounding rock) indicates locally lower stress anisotropy and/or stress magnitudes. The shear velocity anisotropy appears to be caused by the preferential closure of randomly oriented fractures in response to the stress field.

References

Barton, C. A., M. D. Zoback, and D. Moos (1995), Fluid flow along potentially active faults in crystalline rock, *Geology*, *23*, 683–686.

Brace, W. F. (1971), Resistivity of saturated crustal rocks to 40 km based on laboratory measurements, in *The Structure and Physical Properties of the Earth's Crust*, Geophys. Monogr. Ser., vol. 14, edited by J. G. Heacock, pp. 243–255, AGU, Washington, D. C.

Brace, W. F., A. S. Orange, and T. R. Madden (1965), The effect of pressure on electrical resistivity of water saturated crystalline rocks, *J. Geophys. Res.*, *70*, 5669–5678.

Brace, W. F., and A. S. Orange (1968), Further studies of the effect of pressure on electrical resistivity of water saturated crystalline rocks, *J. Geophys. Res.*, *73*, 5407–5420.

Catchings, R. D., et al. (2002), High-resolution seismic velocities and shallow structure of the San Andreas fault zone at Middle Mountain, Parkfield, California, *Bull. Seismol. Soc. Am.*, *92*, 2493–2503.

Chen, S. T. (1988), Shear-wave logging with dipole sources, *Geophysics*, *53*, 659–667.

Crampin, S. (1987), Geological and industrial implications of extensive-dilatancy anisotropy, *Nature*, *328*, 491–496.

Crampin, S., and J. H. Lovell (1991), A decade of shear-wave splitting in the Earth's crust: What does it mean? what use can we make of it? and what should we do next?, *Geophys. J. Int.*, *107*, 387–407.

Crampin, S., R. Evans, and B. K. Atkinson (1984), Earthquake prediction: A new physical basis:, *Geophys. J. R. Astron., Soc.*, *76*, 147–156.

Dahlen, F. A. (1972), Elastic velocity anisotropy in the presence of an anisotropic initial stress, *Bull. Seismol. Soc. Am.*, *62*, 1183–1193.

Ekstrom, M. P., et al. (1987), Formation imaging with microelectrical scanning arrays, *Log Analyst*, *28*, 294–306.

Erzinger, J., T. Wiersberg, and E. Dahms (2004), Real-time mud gas logging during drilling of the SAFOD Pilot Hole in Parkfield, CA, *Geophys. Res. Lett.*, *31*, L15S18, doi:10.1029/2003GL019395.

Hickman, S., and M. D. Zoback (2004), Stress orientations and magnitudes in the SAFOD Pilot Hole, *Geophys. Res. Lett.*, *31*, L15S12, doi:10.1029/2004GL020043.

McPhee, D. K., R. C. Jachens, and C. M. Wentworth (2004), Crustal structure across the San Andreas Fault at the SAFOD site from potential field and geologic studies, *Geophys. Res. Lett.*, *31*, L12S03, doi:10.1029/2003GL019363.

Moos, D., and M. D. Zoback (1983), In situ studies of velocity in fractured crystalline rocks, *J. Geophys. Res.*, *88*, 2345–2358.

Mueller, M. C., A. J. Boyd, and C. Esmeresoy (1994), Case studies of the dipole shear anisotropy log, *SEG Expanded Abstr.*, *64*, 1143–1146.

Nur, A., and G. Simmons (1969), Stress induced velocity anisotropy in rock: An experimental study, *J. Geophys. Res.*, *74*, 6667–6674.

Palacky, G. (1987), Resistivity characteristics of geologic targets, in *Electromagnetic Methods in Applied Geophysics*, edited by M. N. Naibighian, pp. 53, Soc. of Explor. Geophys., Tulsa, Okla.

Pezard, P., and S. M. Luthi (1988), Borehole electrical images in the basement of the Cajon Pass scientific drillhole, California: Fracture identification and tectonic implication, *Geophys. Res. Lett.*, *15*, 1017–1020.

Townend, J., and M. D. Zoback (2000), How faulting keeps the crust strong, *Geology*, *28*, 399–402.

Unsworth, M. J., et al. (2000), Along strike variations in the electrical structure of the San Andreas Fault at Parkfield, California, *Geophys. Res. Lett.*, *27*, 3021–3024.

Williams, C. F., F. V. Grubb, and S. P. Galanis Jr. (2004), Heat flow in the SAFOD pilot hole and implications for the strength of the San Andreas Fault, *Geophys. Res. Lett.*, *31*, L15S14, doi:10.1029/2003GL019352.

Zablocki, C. J. (1964), Electrical properties of serpentinite from Mayaguez, Puerto Rico, in *A Study of Serpentinite*, report, pp. 107–117, Natl. Acad. Sci., Washington, D. C.

————————————

N. L. Boness and M. D. Zoback, Department of Geophysics, Stanford University, CA, USA. (nboness@stanford.edu)